Author Manuscript

**Title:** Highly stable Sr-free cobaltite based perovskite cathodes directly assembled on barrier-layer-free Y2O3-ZrO2 electrolyte of solid oxide fuel cells

**Authors:** Na Ai; Na Li; William Rickard; Yi Cheng; Kongfa Chen; San Ping Jiang, Dr.

# Highly stable Sr-free cobaltite based perovskite cathodes directly assembled on barrier-layer-free $Y_2O_3$-$ZrO_2$ electrolyte of solid oxide fuel cells

Na Ai, ‡[a,b] Na Li, ‡[c] William D.A. Rickard,[d] Yi Cheng,[b] Kongfa Chen,[*,a,b] and San Ping Jiang[*,b]

[a] College of Materials Science and Engineering, Fuzhou University, Fuzhou, Fujian 350108, China

[b] Fuels and Energy Technology Institute and Department of Chemical Engineering, Curtin University, Perth, WA 6102, Australia

[c] College of Science, Heilongjiang University of Science and Technology, Harbin 150022, China

[d] John De Laeter Centre & Department of Physics and Astronomy, Curtin University, Perth, WA 6102, Australia

## Abstract

Direct assembly is a newly developed technique in which cobaltite based perovskite (CBP) cathode can be directly applied to barrier-layer-free $Y_2O_3$-$ZrO_2$ (YSZ) electrolyte with no high temperature pre-sintering steps. Solid oxide fuel cells (SOFCs) based on directly assembled CBPs such as $La_{0.6}Sr_{0.4}Co_{0.2}Fe_{0.8}O_{3-\delta}$ show high performance initially, but degrade rapidly under SOFC operation conditions at 750 $^o$C due to Sr segregation and accumulation at the electrode/electrolyte interface. Herein, we studied systematically the performance and interface of Sr-free CBPs such as $LaCoO_{3-\delta}$ (LC) and $Sm_{0.95}CoO_{3-\delta}$ (SmC) and their

---

[*] Corresponding author. Tel.: +61 8 9266 1723; fax: +61 8 9266 1138.
*Email address*: kongfa.chen@fzu.edu.cn (K. Chen).
[*] Corresponding author. Tel.: +61 8 9266 9804; fax: +61 8 9266 1138.
*Email address*: S.Jiang@curtin.edu.au (S.P. Jiang).
‡These authors contributed equally.

1

composite cathodes directly assembled on YSZ electrolyte. LC electrode undergoes performance degradation and the reason is most likely due to cation demixing and accumulation of lanthanum on YSZ electrolyte under polarization at 500 mAcm$^{-2}$ and 750 $^o$C. On the other hand, the performance and stability of LC electrodes can be substantially enhanced by the formation of LC-GDC composite cathodes. Replacement of La by Sm increased the cell stability and doping of 5% Pd to form $Sm_{0.95}Co_{0.95}Pd_{0.05}O_{3-\delta}$ (SmCPd) significantly improved the electrode activity. An anode-supported YSZ electrolyte cell with a directly assembled SmCPd-GDC composite electrode exhibits a peak power density of 1.4 W cm$^{-2}$ at 750 $^o$C, and an excellent stability at 750 $^o$C for over 240 h. The higher stability of SmC as compared to that of LC is most likely due to the lower reactivity of SmC with YSZ. This study demonstrates the new opportunities in the design and development of intermediate temperature SOFCs based on the directly assembled high performance and durable Sr-free CBP cathodes.

**Keywords**: Solid oxide fuel cells; Sr-free cobaltite based perovskite cathodes; lanthanum segregation; Direct assembly; Polarization induced interface.

## 1. Introduction

Solid oxide fuel cells (SOFCs) are the most efficient fuel cells with low greenhouse gas emission and high fuel flexibility. The state-of-the-art materials of SOFCs are Ni cermet anode, yttria-stabilized zirconia (YSZ) electrolyte and $La_{0.8}Sr_{0.2}MnO_{3+\delta}$ (LSM) cathode. As the operation temperature of SOFCs is reduced from conventional high temperature of 1000 $^o$C to intermediate temperature range of 600-800 $^o$C (intermediate temperature SOFCs, or IT-SOFCs) the polarization losses from the $O_2$ reduction reaction at the cathodes become one of the main performance-limiting factors of IT-SOFCs. In this connection, cobaltite based perovskites (CBPs) such as $La_{0.6}Sr_{0.4}Co_{0.2}Fe_{0.8}O_{3-\delta}$ (LSCF), $Ba_{0.5}Sr_{0.5}Co_{0.2}Fe_{0.8}O_{3-\delta}$ (BSCF),

2

PrBaCo$_2$O$_{5+\delta}$ (PBC) and NdBa$_{0.75}$Ca$_{0.25}$Co$_2$O$_{5+\delta}$ (NBCC) have been extensively investigated as promising cathode materials for IT-SOFCs due to their high mixed ionic and electronic conductivity (MIEC) and high activity for O$_2$ reduction reaction.[1] However, CBPs reacts with YSZ during the conventional electrode high temperature pre-sintering steps, forming insulating phases.[2] To prevent the interaction between CBPs and YSZ YSZ electrolyte, a barrier layer such as Gd or Sm doped ceria is generally used with additional screenprinting and high temperature pre-sintering steps.

Recently we have demonstrated that green CBPs can be directly applied on YSZ electrolyte via a direct assembly approach with no doped ceria interlayer and no conventional high temperature pre-sintering steps.[3] For the directly assembled CBPs, effective electrode/electrolyte interfaces can be formed under the influence of cathodic polarization at a SOFC working temperature of 750 $^o$C. The direct assembly approach significantly simplifies the fabrication processes for SOFCs and most importantly opens the new opportunities of direct application of vast range of CBP cathodes on YSZ electrolyte. In the case of directly assembled CBP cathode such as LSCF on anode supported YSZ electrolyte cells, the cell showed a high peak power density of 1.72 W cm$^{-2}$ at 750 $^o$C.[3c] However, the cell performance is not stable and degrades rather rapidly under the cathodic polarization conditions. Detailed microstructural analysis indicates that performance degradation is caused by the accelerated Sr surface segregation and formation of SrO layer at the LSCF/YSZ interface under the SOFC operation conditions.[4]

Thus, to eliminate the Sr segregation problem we used Sr-free CBPs such as LaCoO$_{3-\delta}$ and SmCoO$_{3-\delta}$ (LC and SmC) directly assembled on YSZ electrolyte cells. LC has a high electrical conductivity exceeding 1000 S cm$^{-1}$ in a temperature range of 500-800 $^o$C,[5] but its ionic conductivity is nearly negligible.[6] The electrocatalytic activity of LC and SmC can be further enhanced by adding an ion conducting component such as gadolinium doped ceria

3

(GDC), similar to the case of LSM and LSCF composite electrodes.[7] The present study shows that a high cell power density and excellent cell operation stability at 750 and 650 $^o$C up to 500 h can be obtained with the directly assembled green LC-GDC and SmC-GDC composite cathodes.

## 2. Experimental

### 2.1. Cell fabrication

NiO-yttria-stabilized zirconia (YSZ) anode-supported YSZ film planar SOFCs were fabricated by slurry spin coating.[8] A bilayer anode structure consisting of a coarse anode support and a fine anode functional layer (AFL) was adopted. The AFL was fabricated without pore-formers to maximize the concentration of reaction sites, while the anode support was fabricated with pore-formers to facilitate the gas diffusion processes. NiO (J.T. Baker), YSZ (TZ-8Y, Tosoh) and tapioca at a weight ratio of 5:5:2.5 were thoroughly blended with isopropanol as media by ball milling. The green anode powder was pressed in a stainless steel die and calcined at 1000 $^o$C for 2 h in air to form the anode substrates. AFL layer of NiO-YSZ (5:5, w/w) and YSZ film were deposited onto the anode substrates using a VTC-100 spin coater (MTI, USA) and co-fired at 1450 $^o$C for 5 h in air. The anode support had dimensions of 14.5 mm in diameter and 0.8 mm in thickness. The thickness of AFL and YSZ layers was 14 and 12 μm, respectively. The gas tightness of YSZ films was verified by microscopic examination as well as by the observation of the cell open circuit voltages as compared to the theoretical values.

$LaCoO_{3-\delta}$ (LC), $Sm_{0.95}CoO_{3-\delta}$ (SmC) and $Sm_{0.95}Co_{0.95}Pd_{0.05}O_{3-\delta}$ (SmCPd) powders were synthesized using modified Pechini approach. Pd was doped in SmC because Pd has been shown to be very effective in promoting the diffusion and exchange process of oxygen species.[9] Stoichiometric $La(NO_3)_3 \cdot 6H_2O$ (99.9%, Alfa-Aesar), $Sm(NO_3)_3 \cdot 6H_2O$ (99%,

4

Sigma-Aldrich), $Co(NO_3)_2 \cdot 6H_2O$ (98.0-102.0%, Alfa-Aesar) and $Pd(NO_3)_2$ (10 wt% aqueous solution, Alfa Aesar) were dissolved in deionized water. Citric acid (99.5%, Chem Supply), ethylenediaminetetraacetic acid (99%, Acros Organics) and ammonia (28%, Ajax Finechem) were added subsequently. The molar ratio of metal ions/citric acid/EDTA was 1:1.5:1. The precursor solution was stirred in a hot plate till it became viscous gel. The gel was dried in oven at 180 $^o$C overnight and the resultant black powder was calcined at 900 $^o$C in air for 2 h. The formation of perovskite phases was examined using a Bruker D8 Advance X-ray diffractometer with a Cu Kα x-ray source.

LC, SmC and SmCPd powders were mixed with ink vehicle (Fuel Cell Materials) at a weight ratio of 5:5 in an agate mortar. The ink was prepared on the YSZ electrolytes by slurry coating and drying at 100 $^o$C for 2 h to form the green electrodes without further pre-sintering at high temperatures. LC-$Gd_{0.1}Ce_{0.9}O_{1.95}$ (GDC, AGC Seimi Chemical Co Ltd), SmC-GDC and SmCPd-GDC composite cathodes were fabricated with 60%CBP and 40%GDC, ball milling for 20 h. The as-prepared composite cathodes were assembled to YSZ electrolyte cells, as described above. The cathode area was 0.25 cm$^2$ and electrode thickness was ~50 μm. Pt ink (Gwent Electronic Materials Ltd) was painted on the electrodes as current collector and heat-treated at 150 $^o$C for 2 h.

2.2. Electrochemical tests

The cell was heated to 750 $^o$C and high purity hydrogen at a flow rate of 50 ml min$^{-1}$ was fed to the anode and the cathode was exposed to the surrounding stationary air. The NiO-YSZ anode was reduced in hydrogen at 750 $^o$C for 1 h prior to the test. Electrochemical polarization curves and impedance spectra were measured in a temperature range of 650-750 $^o$C at an interval of 50 $^o$C using Gamry Reference 3000 Potentiostat. The polarization curves were measured at a scan rate of 5 mV s$^{-1}$. The impedance spectra were measured in a frequency range of 100 kHz–0.1 Hz with a signal amplitude of 10 mV under open circuit

5

conditions. The high frequency intercept of impedance spectra on the real axis represents the cell ohmic resistance, $R_\Omega$, while the difference between the low and high intercepts is related to the electrode polarization resistance, $R_p$. $R_\Omega$ includes the contributions from YSZ electrolyte, electrode and contact resistance between the YSZ and the directly assembled cathode. To investigate the cell stability, cell voltage curves were recorded under a constant current of 500 mA cm$^{-2}$ at 750 $^o$C and 250 mA cm$^{-2}$ at 650 $^o$C. To ensure the reproducibility, at least two cells were tested under identical conditions.

2.3. TEC, microscopic and spectroscopic characterizations

Dense LC and LC-GDC (6/4, w/w) bar samples were prepared for thermal expansion coefficient (TEC) measurements. The powders were compacted at a pressure of 110 MPa to form rectangular bars. LC and LC-GDC bar samples were sintered at 1250 and 1300 ℃ in air for 4 h, respectively. Dimensions of the sintered bar samples were ~13.5 mm×6.8 mm×0.64 mm. The relative density of the sintered LC and LC-GDC bar samples was estimated to be ~95 and 92 %, respectively. TEC measurements were carried out in air from room temperature to 900 $^o$C at a heating rate of 5 $^o$C min$^{-1}$, using a DI-24 Adamel Lhomargy pushrod dilatometer (Roissy En Brie, France) in accordance with ASTM E831. The average TEC of LC from room temperature to 900 $^o$C was 24.0×10$^{-6}$ K$^{-1}$ (Fig. S1, Supporting Information), close to that reported in the literature.[5] This is much higher than the TEC of YSZ, 9.9×10$^{-6}$ K$^{-1}$.[10] The presence of 40 wt% GDC in the LC-GDC composite reduced the TEC to 18.3×10$^{-6}$ K$^{-1}$ (Fig. S1, Supporting Information), due to the lower TEC of GDC, 11.5-11.9×10$^{-6}$ K$^{-1}$.[11] The TEC of SmC was reported to be 24.0×10$^{-6}$ K$^{-1}$,[12] identical to that of LC.

The microstructure of the cells was examined using scanning electron microscopy (SEM, Zeiss NEON 40EsB). The directly assembled cathodes were removed from the YSZ films by adhesive tape, and the elemental distribution on the YSZ surface was analysed by time of

6

flight secondary ion mass spectroscopy (ToF-SIMS) in a Tescan Lyra3 focused ion beam-SEM (FIB-SEM). ToF-SIMS was conducted over a 5 x 5 µm area using a $Ga^+$ ion beam accelerating voltage of 30 kV and current of 35 pA. A lamella at the electrode/electrolyte surface was also prepared in the FIB-SEM. Microstructural observation and elemental mapping analysis of the lamella were characterized using high angle annular dark field scanning transmission electron microscopy (HAADF-STEM, FEI Titan G2 80-200 TEM/STEM with ChemiSTEM Technology) at 200 kV. In some cases, the cathodes were removed from the YSZ surface by acid treatment in 32% HCl solution for 24 h. The acid cleaned YSZ surface was examined using a Bruker Dimension FastScan atomic force microscope (AFM) in tapping mode. X-ray photoelectron spectroscopy (XPS) was carried out on as prepared and polarized SmCPd-GDC cathodes using a Kratos AXIS Ultra DLD system, with monochromated Al Kα X-rays (photon energy 1486.7 eV) at a pass energy of 40 eV.

## 3. Results and discussion

### 3.1. XRD and chemical reactivity of LC and SmC

Fig. 1a shows the XRD patterns of LC, SmC and SmCPd powders calcined at 900 $^o$C. The XRD patterns show the perovskite structure with no other phases, indicating the formation of perovskite phases of the powders. The chemical activity of LC-YSZ and SmC-YSZ oxide couples was studied and the results are shown in Fig. 1b. LC-YSZ is chemically compatible at 800 $^o$C, but a secondary phase, $La_2Zr_2O_7$, was detected at 850 $^o$C. This indicates that the reactivity between LC and YSZ would be very small or negligible at temperatures lower than 800 $^o$C. In the case of SmC-YSZ oxide couple, secondary phases, $Sm_{0.33}Zr_{0.67}O_{1.83}$ and/or $Co_3O_4$, were formed at 900 $^o$C and above, higher than 800 and 850 $^o$C in the case of LSCF-YSZ[3c] and LC-YSZ, respectively. This indicates the better chemical compatibility of SmC with YSZ as compared to that between LC and YSZ. Tu et al. studied

7

the chemical compatibility of SmC powder prepared by solid state reaction and reported that SmC is chemically stable with YSZ at temperatures as high as 1000 $^{o}$C for 96 h.[12]

Fig. 1c and d show the SEM micrographs of directly assembled green LC, LC-GDC, SmC and SmC-GDC composite electrodes. LC electrode is porous with an average particle size of 0.47±0.16 μm (Fig. 1c). In the case of the LC-GDC electrode, there are randomly distributed smaller GDC particles in the size range of 0.07-0.38 μm in addition to the large LC particles (Fig. 1c). SmC electrode had a particle size of 0.37±0.16 μm and the GDC particles distributed uniformly in the SmC-GDC composite electrode (Fig. 1d), similar to that of LC-GDC composite electrode.

## 3.2. Performance and stability of cells with directly assembled LC and LC-GDC electrodes

Fig. 2 is the polarization curves and impedance spectra of an anode-supported YSZ electrolyte cell with a directly assembled LC cathode as a function of polarization time at 500 mA cm$^{-2}$, 750 $^{o}$C. The initial peak power density (PPD) was 0.25 W cm$^{-2}$ and increased quickly to 0.53 W cm$^{-2}$ after polarization for 20 h (Fig. 2a). The increase of PPDs corresponds to the substantial decrease in the cell ohmic and electrode polarization resistances, $R_\Omega$ and $R_p$, respectively. The initial $R_\Omega$ and $R_p$ were 0.56 and 40.87 $\Omega$ cm$^{2}$, respectively, and decreased to 0.11 and 2.92 $\Omega$ cm$^{2}$ after polarization for 20 h (Fig. 2b). The cell voltage was 0.38 V and increased rapidly to 0.73 V after polarization for 10 h; the cell voltage was stable for ~40 h, followed by a quick decline with the further polarization (Fig.2c). The cell voltage was reduced to 0.54 V after polarization for 100 h. It is interesting to note that polarization performance can be recovered after the interruption of polarization current. This probably explains the relatively small differences of the polarization curves measured after the cell was polarized for 20 h and 100 h as the polarization curves were obtained after the recovery of the polarization performance. The exact reason for the performance recovery on assembled green LC cathode is not clear at this stage. Nevertheless,

8

the polarization performance degrades very rapidly after the application of the current (Fig.2c). The performance decay was mainly due to the increase of $R_p$, as $R_\Omega$ was unchanged after polarization for 20 h (see the inset of Fig. 2b). This shows that the directly assembled Sr-free LC electrode is not stable under polarization conditions. We also tested the cell under open circuit conditions at 750 $^o$C for 250 h and found there was no change in the cell polarization performance. This indicates that the polarization is the major cause contributing to the performance decay of green LC electrode.

Fig. 3a and b show the polarization curves and impedance spectra of the directly assembled LC-GDC composite cathode as a function of polarization time at 500 mA cm$^{-2}$, 750 $^o$C. The initial PPD was 0.45 W cm$^{-2}$ and increased quickly with the elapsed polarization time (Fig. 3a). For example, after polarization for 4, 20 and 150 h, the PPDs increased to 0.62, 1.05 and 1.21 W cm$^{-2}$, respectively. The increase of PPDs corresponded to the substantial decrease in both $R_\Omega$ and $R_p$. The initial $R_\Omega$ and $R_p$ were 0.26 and 0.82 $\Omega$ cm$^2$ and decreased to 0.06 and 0.58 $\Omega$ cm$^2$, respectively, after polarization for 150 h (Fig. 3b). The drastic reduction of $R_\Omega$ indicates the formation of electrode/electrolyte interface under the influence of polarization.[3a] The cell performance was also measured at different temperatures and PPDs were 1.14 and 0.73 and 0.39 W cm$^{-2}$ at 750, 700 and 650 $^o$C, respectively (Fig. 3c). In this case, a new cell with directly assembled green LC-GDC composite cathode was polarized at 500 mA cm$^{-2}$, 750 $^o$C for 20 h before the measurements.

Fig. 4 shows the stability curves and the corresponding impedance spectra of cells with the directly assembled LC-GDC electrodes under constant currents. For the cell polarized at 500 mA cm$^{-2}$ and 750 $^o$C, the cell voltage increased rapidly in the first 20 h and then became almost stable, but after polarization for 150 h the cell voltage started to decline gradually (Fig. 4a). The cell voltage was 0.86 V after polarization for 150 h and decreased to 0.81 V with further polarization for 250 h. The cell degradation is most likely caused by the increase of

9

$R_\Omega$ (indicated by the arrow, Fig. 4c). $R_\Omega$ and $R_p$ were 0.06 and 0.58 $\Omega$ cm$^2$ after polarization for 150 h and increased to 0.09 and 0.63 $\Omega$ cm$^2$ after polarization for 250 h. Nevertheless, the cells with directly assembled LC-GDC composite cathodes are much more stable than those with directly assembled LC and LSCF electrodes. In the case of the directly assembled LSCF electrode tested under identical conditions, the performance decreased significantly with the polarization time after the PPD reached a maximum in the first 6 h.[4]

The stability of cells with directly assembled LC-GDC cathode was also tested at a reduced temperature of 650 °C. The cell was polarized at 500 mA cm$^{-2}$ and 750 °C for 20 h prior to the stability test. During the stability test at 650 °C, the cell voltage initially experienced a decrease up to 100 h, but overall the cell shows an excellent stability at 250 mA cm$^{-2}$ and 650 °C for 500 h, despite the increase of the $R_p$ (Fig. 4d). Different to that observed at 750 °C, the cell ohmic resistance is stable, indicating the very stable LC-GDC/YSZ interface under the polarization conditions at 650 °C.

## 3.3. LC/YSZ and LC-GDC/YSZ interface

Fig. 5 shows the SEM micrographs of YSZ electrolyte after the directly assembled LC electrode was polarized at 500 mA cm$^{-2}$ and 750 °C for 100 h. LC electrode was removed by adhesive tape. On the electrolyte surface were a number of irregularly shaped particles (Fig. 5a), i.e., plate-like or layer-shaped large particles in the size range of 0.35-3.2 μm (spot 2, Fig. 5b), particles with clear crystalline facets in the size range of 140-550 nm (spot 3, Fig. 5b), and small particles in the size range of 40-110 nm (spot 1, Fig. 5c). EDS analysis indicate that the layer-shaped large particles consist of metallic Pt, Co and Ni (spot 2, Fig. 5e), while the particles with crystalline facets contain primarily Co (spot 3, Fig. 5f), indicating the formation of cobalt oxides, CoO or $Co_3O_4$. Nano-sized particles also contain Co and Ni (spot 1, Fig. 5e). The Ni species may come from the Ni-YSZ anode side. Zhou et al studied the electrochemical performance of LSM cathodes on Ni-YSZ anode supported thin YSZ

10

electrolyte cells and observed the Ni diffusion from the anode side to the LSM cathodes, varying in the range of 1.2 to 2.5 at% Ni at the LSM cathode layer.[13] The presence of Ni caused the densification of the LSM microstructure. Ni diffusion into YSZ electrolyte most likely occurred during the high temperature sintering of the anode supported cells as Ni has certain solubility in YSZ at temperatures of 1450 $^{\circ}$C.[14] On the other hand, YSZ electrolyte surface in contact with a directly assembled LC electrode after heat-treatment at 750 $^{\circ}$C for 250 h under open circuit conditions is very clean and the particles on the YSZ electrolyte surface are most likely LC particles (spot 4, Fig. 5f). The presence of Co-containing particles (large particle with clear crystalline facets and nano-sized particles) indicates the deposition of cobalt species at the interface under the influence of polarization. Nano-sized particles were also observed on the YSZ electrolyte surface in contact with a directly assembled LC after polarization for 12 h (Fig.5g and h). As shown in Fig.5h, treatment in HCl acid solutions cannot remove the deposited particles, indicating the possible reaction between the deposited particles and YSZ electrolyte under SOFC operation conditions.

Fig. 6 shows the ToF-SIMS and STEM analysis at the electrode/electrolyte interface of a directly assembled LC electrode after polarization at 750 $^{\circ}$C for 100 h. On a typical electrolyte surface region with large and small particles (Fig. 6a), Co and in particular La are enriched on the YSZ surface (Fig. 6b). The La enrichment mainly occurred on the top ~20 nm YSZ surface, while the Co-rich layer was ~40 nm in depth. The elemental maps show La was uniformly dispersed (Fig. 6c), while Co mainly existed in discrete particles (Fig. 6d). Thus it is clear that the small particles observed by SEM (see Fig. 6a) are related to the deposited La species. There are significant particle deposition and formation on the YSZ electrolyte surface in contact with the directly assembled LC cathode after polarization at 750 $^{\circ}$C for 100 h and deposited particles cannot be removed by HCl treatment (Fig.S2, Support Information). The formation of $La_2Zr_2O_7$ phase may be possible as $La_2Zr_2O_7$ has been

11

extensively observed as the reaction product between La-containing perovskites and YSZ electrolyte.[15]

A lamella was also prepared from the LC electrode/YSZ electrolyte interface and the elemental maps showed the formation of a distinctive Pt layer at the interface (Fig. 6e), consistent with the EDS observations (see Fig. 5e). The deposition of Pt is attributed to the use of Pt ink as current collector and this phenomenon was also reported by others.[16] La surface segregation was clearly observed on the LC particles (indicated by the arrows, Fig. 6e). The extraction of La would induce partial decomposition of the LC structure, as evident by the observation of Co-rich particles (Fig. 5 and Fig. 6d). The presence of electrochemically inert La species and possible formation of insulating phase at the interface can block the active surface area for the oxygen reduction reaction on LC electrode, leading to the deterioration of electrode activity and thereby cell degradation as observed in this study.

Fig. 7 shows the SEM micrographs of the cell with a directly assembled LC-GDC cathode after polarization at $750\,^{o}C$ for 250 h. The cathode was partially peeled off during the cell disassembly process, but there was a thin electrode layer attached to the electrolyte (indicated by the arrows, Fig. 7a). The existence of the electrode layer was clearly observable from the top view of the electrolyte surface (Fig. S3a, Supporting Information). In the case of a directly assembled green LC-GDC electrode after treatment under identical conditions but without passing current, the YSZ electrolyte surface was much cleaner (Fig.S3b, Supporting Information). This indicates the significant effect of polarization on the interface contact between directly assembled cathode and YSZ electrolyte. Ring shaped contact marks were formed on the YSZ surface after polarization for only 40 h (indicated by the arrows in Fig. 7b and AFM images in Fig. 7c and d). The contact marks are convex rings in the size of $91\pm27$ nm (Fig.7d). The rings have an edge width of ~32 nm and a height of 5-10 nm (Fig. 7e). Contact rings were also formed after the stability test at $650\,^{o}C$ for 500 h (Fig. S4, Supporting

12

Information). These contact rings look very similar to the rings formed on YSZ electrolyte surface in contact with pre-sintered LSM electrode.[3a, 17] The formation of these contact rings and marks indicates the formation of electrode/electrolyte interface under the influence of polarization, consistent with the substantial decrease of $R_\Omega$ and $R_p$ during the early stage of polarization of the cells at 750 °C (Fig. 3b).

The much cleaner YSZ electrolyte surface in contact with directly assembled LC-GDC composite electrode as compared to that with the LC electrode indicates the addition of GDC substantially suppresses the La extraction and enhances the stability of LC under the influence of polarization. This is consistent with the much better stability of LC-GDC electrode than that of pristine LC electrode (see Fig.4). Adding GDC to form the LC-GDC composite electrode significantly enhances the electrode activity and reduces the cathodic overpotential, leading to the substantially reduced La extraction and in turn enhancing the structural stability and electrochemical performance of LC electrode.

## 3.5. Performance of cells with directly assembled SmC and SmCPd electrodes

Fig. 8 is the polarization curves and impedance spectra of a cell with a directly assembled SmC electrode at 750 °C under currents of 100 mA cm$^{-2}$ for 20 h and 500 mA cm$^{-2}$ for 100 h. The cell performance was substantially enhanced by the polarization and became very stable for 120 h (Fig. 8a and c). The initial PPD was 0.07 W cm$^{-2}$ and increased to 0.35 W cm$^{-2}$ after polarization for 120 h. The performance enhancement is related to the reduction of $R_\Omega$ and in particular $R_p$ (Fig.8b). In contrast to the directly assembled LC electrode (see Fig.2c), the cell with directly assembled SmC cathode is very stable (Fig.8c). After the application of polarization current, the cell voltage recovered rapidly to the original value before the current interruption (Fig.8c). This is very different to the rapid performance decay in the case of LC electrode (Fig. 2c). After removal of the directly assembled green SmC electrode, the electrolyte surface was quite clean (Fig. 8d), which is very different to the

13

significant particle formation on the YSZ surface in contact with the directly assembled LC electrode (see Fig. 5). This indicates that the SmC has a much better stability as compared to the LC.

The polarization and impedance performance of a cell with directly assembled SmC-GDC composite electrode were also studied at 500 mA cm$^{-2}$ and 750 $^{o}$C and the results are shown in Fig. 9a and b. The polarization current has a substantial promotion effect on the cell performance. The initial PPD was 0.35 W cm$^{-2}$, and increased to 0.52, 0.60 and 0.77 W cm$^{-2}$ after polarization for 4, 20 and 150 h, respectively (Fig. 9a). The cell voltage also increased rapidly in the first 20 h followed by a gradual increase with further polarization for 225 h (Fig. 9b). Similar to the case of directly assembled LC-GDC electrode, the increase of cell performance is attributable to the decrease of $R_{\Omega}$ and $R_p$. The initial $R_{\Omega}$ and $R_p$ were 0.45 and 0.82 $\Omega$ cm$^2$, respectively, and decreased to 0.13 and 0.81 $\Omega$ cm$^2$ after polarization for 150 h (see the inset of Fig. 9b). Nevertheless, the overall performance of the directly assembled SmC-GDC electrode is lower than that of LC-GDC electrodes.

The electrocatalytic activity of SmC cathodes is enhanced by doping of small amount of Pd. The initial PPD of a cell with directly assembled SmCPd-GDC cathode was 0.58 W cm$^{-2}$ and increased rapidly to 1.40 W cm$^{-2}$ after polarization for 150 h (Fig. 9c), significantly higher than 0.77 W cm$^{-2}$ with the SmC-GDC electrode (Fig. 9a). This indicates that the doping of a small amount of Pd is highly effective in enhancing the electrocatalytic activity of SmC electrode. The improvement of cell performance by the polarization is attributed to the decrease of $R_{\Omega}$ and $R_p$ (see the inset of Fig. 9d). The initial $R_{\Omega}$ and $R_p$ were 0.17 and 0.47 $\Omega$ cm$^2$ and decreased to 0.09 and 0.39 $\Omega$ cm$^2$, respectively, after polarization for 150 h. Similar to the case of the SmC-GDC electrode, the cell with the directly assembled SmCPd-GDC electrode is very stable at 500 mA cm$^{-2}$ for over 240 h (Fig. 9d).

3.5. SmCPd-GDC/YSZ interface

14

Fig. 10 shows an AFM image and height profiles of YSZ electrolyte surface of the cell with the directly assembled SmCPd-GDC electrode after polarized at 500 mA cm$^{-2}$ and 750 $^{o}$C for 240 h. The SmCPd-GDC cathode was removed by HCl treatment. Island like contact marks surrounded by trenches were observed on the YSZ electrolyte surface (Fig. 10a). The contact islands are ~120 nm in diameter and the trenches are 2-3 nm in depth (Fig. 10b). Some contact marks are ring-shaped and the edge has a height of ~4 nm (see height profile 2, Fig. 10b). The morphology of these contact marks is different to that formed in the case of LC-GDC electrodes (Fig. 7c and d), implying the microstructure of contact marks may be dependent on the composition of cathode materials. Nevertheless, the observation of contact marks again confirms the formation of electrode/electrolyte interface, consistent with the substantial decrease of R$_\Omega$ (see Fig. 9d).

XPS was conducted to study Pd 3d core levels on the directly assembled SmCPd-GDC electrodes (see Fig. 10c). For the as prepared electrode, Pd 3d$_{5/2}$ occurred at 337.2 eV, which is higher than ~335.0 and ~336.4 eV of Pd 3d$_{5/2}$ in Pd and PdO, respectively.[18] This indicates that Pd most likely existed in the B-site of the SmC perovskite structure. After polarization at 500 mA cm$^{-2}$ and 750 $^{o}$C for 160 h, in addition to the peak at 337.2 eV, a new Pd 3d$_{5/2}$ peak occurred at a lower binding energy of 336.4 eV, which can be assigned to PdO.[18] This indicates that PdO may be partially exsolved from the SmCPd lattice. The exsolution of highly active PdO on the surface of SmCPd-GDC electrode could promote the ORR,[19] leading to the enhanced electrochemical activity of the SmCPd electrode and therefore substantially enhanced cell performance. This is consistent with the significant promotion effect of Pd/PdO on the surface diffusion and exchange process of oxygen species for the oxygen reduction reaction.[9, 20]

Very different from the widely reported Sr segregation in Sr-containing CBPs based oxygen separation membranes and oxygen electrodes,[21] lanthanum in the perovskite

15

structure is generally stable and there is almost no report on the surface segregation and diffusion of La under SOFC operation conditions. La segregation and diffusion could occur in the presence of impurities such as chromium and boron under the polarization conditions due to the formation of lanthanum chromite or borate.[22] In the present study, La segregation or extraction was clearly observed on the directly assembled green LC electrode, leading to the decomposition of LC and deposition of Co- and La-containing particles on the YSZ electrolyte surface. Such La extraction and formation of Co- and La-containing particles on the YSZ electrolyte surface may indicate the occurrence of kinetic or cation demixing of LC under the SOFC operation conditions.[23] The presence of La and increase of $R_\Omega$ of the cell with directly assembled LC-GDC composite cathode indicates the possible formation of resistive $La_2Zr_2O_7$ at the LC/YSZ interface. Sahu et al studied formation enthalpy and thermodynamic stability of lanthanide cobalt perovskites, $LnCoO_{3-\delta}$ (Ln = La, Nd, Sm, Gd) and found that these perovskites become energetically less stable with the decrease of ionic radius of the lanthanide (from La to Gd).[24] The tolerance factor of SmC is 0.94, lower than 0.97 of LC, indicating that LC is thermodynamically more stable than SmC. However, in this study, the directly assembled SmC electrode showed a significantly better stability as compared to the directly assembled LC electrode under SOFC operation conditions. The reason for the better stability of directly assembled SmC electrodes on YSZ electrolyte is most likely due to the better chemical compatibility between SmC and YSZ, as shown in the oxide couples studies (Fig.1). This is consistent with the better chemical stability of SmC with YSZ than that of LC with YSZ reported by Tu et al.[12]. The good stability of directly assembled LC electrode under open circuit conditions indicates that polarization plays an important role to accelerate La extraction and accumulation on the YSZ surface. The addition of ionic conducting GDC phase to form LC-GDC composite substantially increases the electrochemical activity of LC for the $O_2$ reduction reaction, reducing the driving force for

16

the La extraction and thus enhancing the activity and stability of directly assembled LC electrodes. This indicates that in addition to the thermodynamical considerations, the kinetic issues such as polarization and chemical compatibility also play a critical role in the cation segregation or extraction of the CBPs. However, more systematic studies are required to understand the fundamental relationship between the surface segregation, diffusion, energetics and chemical compatibility of directly assembled green CBP electrode and YSZ electrolyte under SOFC operation conditions.

Deposition of Pt at the electrode/electrolyte interface is a common phenomenon under SOFC operation conditions.[16] The deposited Pt may initially promote the electrocatalytic activity of assembled electrode, however, the performance and stability of cells with various directly assembled cathodes are related directly to the nature of the cathodes as shown in this study. This indicates that effect of the deposited Pt from Pt current collector on the cell performance and stability is generally small or at least does not play a dominant role in the electrode activity and stability under conditions of the present study.

## 4. Conclusions

Sr-free LC and SmC and their composite cathodes were applied to YSZ electrolyte by a direct assembly approach and the cell performance and interface microstructure were studied in detail. The Ni-YSZ anode supported YSZ electrolyte cells with directly assembled LC electrode showed significant improvement in the performance under SOFC operation conditions and the PPD increased from 0.25 W cm$^{-2}$ to 0.53 W cm$^{-2}$ after polarization at 500 mA cm$^{-2}$ and 750 $^{o}$C for 20 h. However, the directly assembled LC was not stable and microstructural analysis indicated the cation demixing and subsequent formation of Co and La-rich particles on the YSZ electrolyte surface under the influence of polarization, leading to partial decomposition of LC perovskite structure and degradation of the cell. The addition of GDC to form LC-GDC composite cathodes substantially enhanced the performance and

17

stability of the directly assembled LC-GDC cathodes. A cell with a directly assembled LC-GDC composite cathode demonstrated a PPD of 1.21 W cm$^{-2}$ at 750 $^{o}$C and an excellent stability at 650 $^{o}$C for 500 h. The stability of Sr-free CBP electrodes can be significantly enhanced by replacing La with Sm to form SmC electrode. Under identical polarization conditions, the YSZ electrolyte surface was much cleaner and showed no visible deposition of Sm- or Co-containing particles. The significantly better stability of the directly assembled SmC electrode as compared to that of LC electrode under SOFC operation conditions is due to the better chemical compatibility between SmC and YSZ. The electrocatalytic activity of SmC cathode was further improved by doping 5% Pd, forming SmCPd. The cell with the directly assembled SmCPd-GDC composite electrode not only exhibited a high PPD of 1.4 W cm$^{-2}$ at 750 $^{o}$C, but also showed excellent stability at 750 $^{o}$C for 240 h under a current density of 500 mA cm$^{-2}$. XPS analysis indicated the possible Pd exsolution under the cathodic polarization conditions, which may be responsible for the significantly enhanced electrode activity and cell power density.

One of the most significant findings of the present study is the observation of La extraction of lanthanum cobalt perovskites and Pd exsolution under the influence of cathodic polarization conditions. Though the exact reasons are not known at this stage, the findings open up new opportunities in the engineering and design of directly assembled Sr-free CBP electrode materials with high activity and stability for IT-SOFCs.

**Acknowledgements**

18

Microanalysis Facility and the Australian Microscopy & Microanalysis Research Facility at the Centre for Microscopy, Characterisation & Analysis, The University of Western Australia, both of which are partially funded by the University, State and Commonwealth Governments, the WA X-Ray Surface Analysis Facility, funded by the Australian Research Council LIEF grant (LE120100026), and the Department of Chemistry/Nanochemistry Research Institute, Curtin University.

## References

[1]     aK. Murata, T. Fukui, H. Abe, M. Naito, K. Nogi, *Journal of Power Sources* **2005**, *145*, 257; bS.-W. Baek, J. Jeong, Y.-M. Kim, J. H. Kim, S. Shin, J. Bae, *Solid State Ionics* **2011**, *192*, 387; cC. Su, X. Xu, Y. Chen, Y. Liu, M. O. Tadé, Z. Shao, *Journal of Power Sources* **2015**, *274*, 1024; dS. Yoo, A. Jun, Y. W. Ju, D. Odkhuu, J. Hyodo, H. Y. Jeong, N. Park, J. Shin, T. Ishihara, G. Kim, *Angewandte Chemie International Edition* **2014**, *53*, 13064; eL. Zhu, B. Wei, Z. Wang, K. Chen, H. Zhang, Y. Zhang, X. Huang, Z. Lü, *ChemSusChem* **2016**, *9*, 2443.
[2]     O. Yamamoto, Y. Takeda, R. Kanno, M. Noda, *Solid State Ionics* **1987**, *22*, 241.
[3]     aS. P. Jiang, *Journal of The Electrochemical Society* **2015**, *162*, F1119; bM. Li, K. Chen, B. Hua, J.-l. Luo, W. D. A. Rickard, J. Li, J. T. S. Irvine, S. P. Jiang, *Journal of Materials Chemistry A* **2016**, *4*, 19019; cK. Chen, N. Li, N. Ai, M. Li, Y. Cheng, W. D. A. Rickard, J. Li, S. P. Jiang, *Journal of Materials Chemistry A* **2016**, *4*, 17678.
[4]     K. Chen, N. Li, N. Ai, Y. Cheng, W. D. A. Rickard, S. P. Jiang, *ACS Applied Materials & Interfaces* **2016**, *8*, 31729.
[5]     Y. Ohno, S. Nagata, H. Sato, *Solid State Ionics* **1983**, *9–10, Part 2*, 1001.
[6]     aC. H. Chen, H. Kruidhof, H. J. M. Bouwmeester, A. J. Burggraaf, *J. Appl. Electrochem.* **1997**, *27*, 71; bW. Zhou, Z. Shao, R. Ran, P. Zeng, H. Gu, W. Jin, N. Xu, *Journal of Power Sources* **2007**, *168*, 330.
[7]     aS. P. Jiang, W. Wang, *J. Electrochem. Soc.* **2005**, *152*, A1398; bK. T. Lee, A. A. Lidie, H. S. Yoon, E. D. Wachsman, *Angewandte Chemie* **2014**, *126*, 13681; cT. E. Burye, J. D. Nicholas, *J. Power Sources* **2016**, *301*, 287; dA. Esquirol, N. P. Brandon, J. A. Kilner, M. Mogensen, *J. Electrochem. Soc.* **2004**, *151*, A1847; eT. Tsai, S. A. Barnett, *Solid State Ionics* **1997**, *93*, 207; fF. Bidrawn, J. M. Vohs, R. J. Gorte, *J. Electrochem. Soc.* **2010**, *157*, B1629.
[8]     aK. F. Chen, Z. Lu, N. Ai, X. Q. Huang, Y. H. Zhang, X. D. Ge, X. S. Xin, X. J. Chen, W. H. Su, *Solid State Ionics* **2007**, *177*, 3455; bK. F. Chen, X. J. Chen, Z. Lu, N. Ai, X. Q. Huang, W. H. Su, *Electrochimica Acta* **2008**, *53*, 7825.
[9]     aF. L. Liang, J. Chen, J. L. Cheng, S. P. Jiang, T. M. He, J. Pu, J. Li, *Electrochem. Commun.* **2008**, *10*, 42; bT. H. Shin, Y. Okamoto, S. Ida, T. Ishihara, *Chemistry–A European Journal* **2012**, *18*, 11695; cD. M. Bierschenk, E. Potter-Nelson, C. Hoel, Y. G. Liao, L. Marks, K. R. Poeppelmeier, S. A. Barnett, *J. Power Sources* **2011**, *196*, 3089.
[10]    M. B. Phillipps, N. M. Sammes, O. Yamamoto, *Solid State Ionics* **1999**, *123*, 131.
[11]    V. V. Kharton, F. M. Figueiredo, L. Navarro, E. N. Naumovich, A. V. Kovalevsky, A. A. Yaremchenko, A. P. Viskup, A. Carneiro, F. M. B. Marques, J. R. Frade, *J. Mater. Sci.* **2001**, *36*, 1105.
[12]    H. Tu, Y. Takeda, N. Imanishi, O. Yamamoto, *Solid State Ionics* **1997**, *100*, 283.
[13]    X. D. Zhou, S. P. Simner, J. W. Templeton, Z. Nie, J. W. Stevenson, B. P. Gorman, *J. Electrochem. Soc.* **2010**, *157*, B643.
[14]    aA. Kuzjukevics, S. Linderoth, *Solid State Ionics* **1997**, *93*, 255; bS. Linderoth, N. Bonanos, K. V. Jensen, J. B. Bilde-Sørensen, *Journal of the American Ceramic Society* **2001**, *84*, 2652; cG. Stefanic, M. Didovic, S. Music, *J. Mol. Struct.* **2007**, *834*, 435; dH. Kondo, T. Sekino, T. Kusunose, T. Nakayama, Y. Yamamoto, K. Niihara, *Mater. Lett.* **2003**, *57*, 1624.
[15]    D. Chen, F. Wang, Z. Shao, *International Journal of Hydrogen Energy* **2012**, *37*, 11946.
[16]    aS. P. Simner, M. D. Anderson, L. R. Pederson, J. W. Stevenson, *Journal of The Electrochemical Society* **2005**, *152*, A1851; bY. Xiong, K. Yamaji, H. Kishimoto, M. E. Brito, T. Horita, H. Yokokawa, *Electrochemical and Solid-State Letters* **2009**, *12*, B31.
[17]    aA. Mitterdorfer, L. J. Gauckler, *Solid State Ionics* **1998**, *111*, 185; bT. Horita, T. Tsunoda, K. Yamaji, N. Sakai, T. Kato, H. Yokokawa, *Solid State Ionics* **2002**, *152–153*, 439; cK. Chen, S.-S. Liu, N. Ai, M. Koyama, S. P. Jiang, *Physical Chemistry Chemical Physics* **2015**, *17*, 31308; dN. Li, N. Ai, K. Chen, Y. Cheng, S. He, M. Saunders, A. Dodd, A. Suvorova, S. P. Jiang, *RSC Advances* **2016**, *6*, 99211.
[18]    aE. H. Voogt, A. J. M. Mens, O. L. J. Gijzeman, J. W. Geus, *Surface Science* **1996**, *350*, 21; bM. Brun, A. Berthet, J. C. Bertolini, *Journal of Electron Spectroscopy and Related Phenomena* **1999**, *104*, 55.
[19]    aF. L. Liang, J. Chen, S. P. Jiang, B. Chi, J. Pu, L. Jian, *Electrochem. Commun.* **2009**, *11*, 1048; bK. Chen, N. Ai, S. P. Jiang, *International Journal of Hydrogen Energy* **2012**, *37*, 1301.
[20]    J. Chen, F. L. Liang, B. Chi, J. Pu, S. P. Jiang, L. Jian, *J. Power Sources* **2009**, *194*, 275.

19

[21]    aM. M. Viitanen, R. G. von Welzenis, H. H. Brongersma, F. P. F. van Berkel, *Solid State Ionics* **2002**, *150*, 223; bM. M. Viitanen, R. G. V. Welzenis, H. H. Brongersma, F. P. F. Van Berkel, *Solid State Ionics* **2002**, *150*, 223; cS. P. Simner, M. D. Anderson, M. H. Engelhard, J. W. Stevenson, *Electrochemical and Solid-State Letters* **2006**, *9*; dL. Zhao, J. Drennan, C. Kong, S. Amarasinghe, S. P. Jiang, *Journal of Materials Chemistry A* **2014**, *2*, 11114; eD. Oh, D. Gostovic, E. D. Wachsman, *J. Mater. Res.* **2012**, *27*, 1992.

[22]    aV. I. Sharma, B. Yildiz, *Journal of the Electrochemical Society* **2010**, *157*, B441; bK. Chen, L. Fang, T. Zhang, S. P. Jiang, *Journal of Materials Chemistry A* **2014**, *2*, 18655; cK. Chen, S.-S. Liu, P. Guagliardo, M. R. Kilburn, M. Koyama, S. P. Jiang, *J. Electrochem. Soc.* **2015**, *162*, F1282; dK. Chen, J. Hyodo, N. Ai, T. Ishihara, S. P. Jiang, *Int. J. Hydrog. Energy* **2016**, *41*, 1419.

[23]    aF. Tietz, W. Jungen, P. Lersch, M. Figaj, K. D. Becker, *Chem. Mat.* **2002**, *14*, 2252; bL. Baque, A. Soldati, H. Troiani, A. Serquis, in *Solid State Ionic Devices 10*, Vol. 64 (Eds: E. Traversa, G. Jackson, A. Herring, A. Wachsman, R. Mukundan, P. Vanysek),  2014, 11.

[24]    S. K. Sahu, S. Tanasescu, B. Scherrer, C. Marinescu, A. Navrotsky, *Journal of Materials Chemistry A* **2015**, *3*, 19490.

20
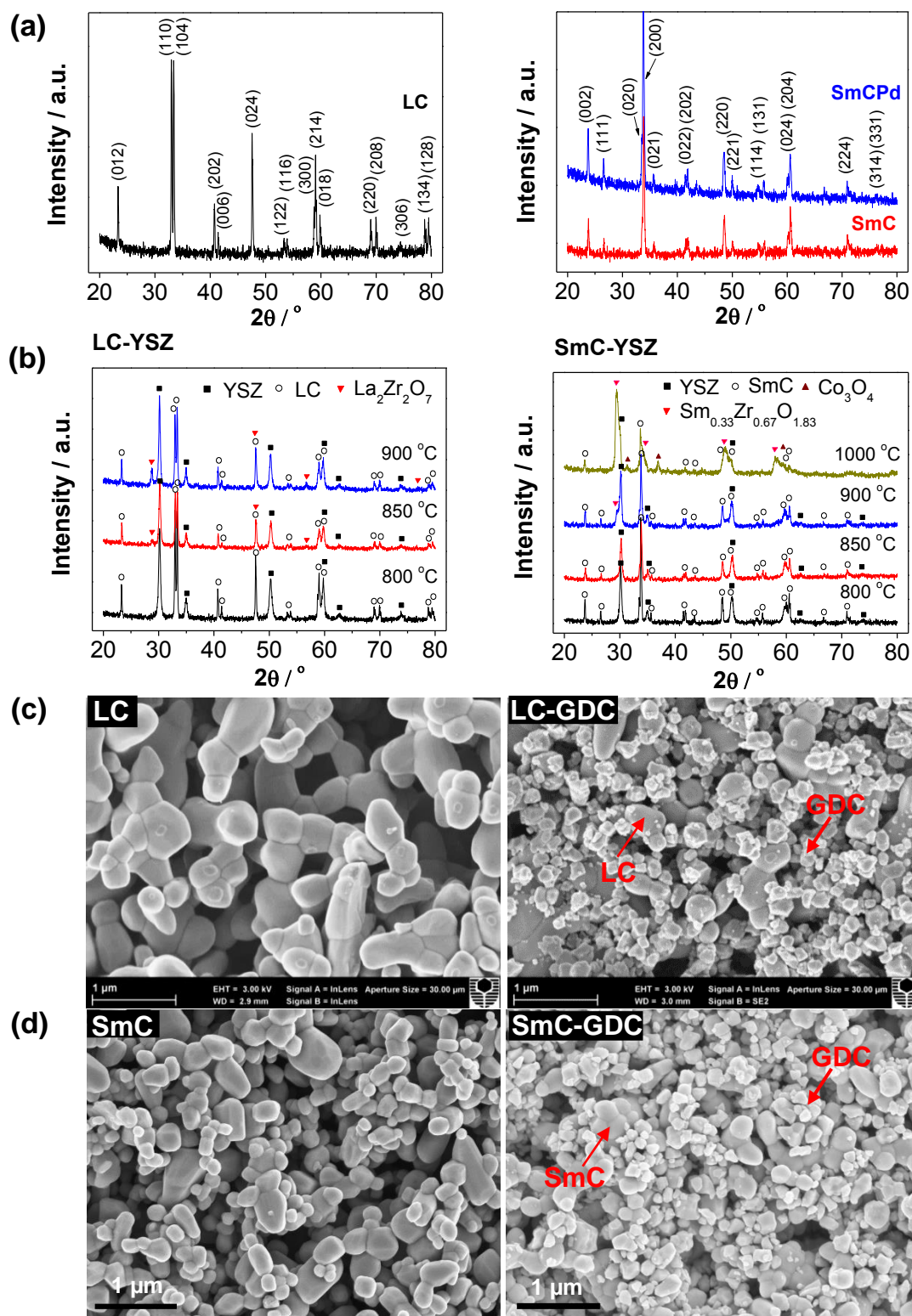
**Figure 1**. (a) XRD patterns of as-prepared LC, SmC and SmCPd powders, (b) XRD patterns of LC-YSZ couples calcined at 800-900 °C for 4 h and SmC-YSZ couples calcined at 800-1000 °C for 4 h. SEM micrographs of the surface of directly assembled cathodes: (c) LC and LC-GDC composite, and (d) SmC and SmC-GDC composite.
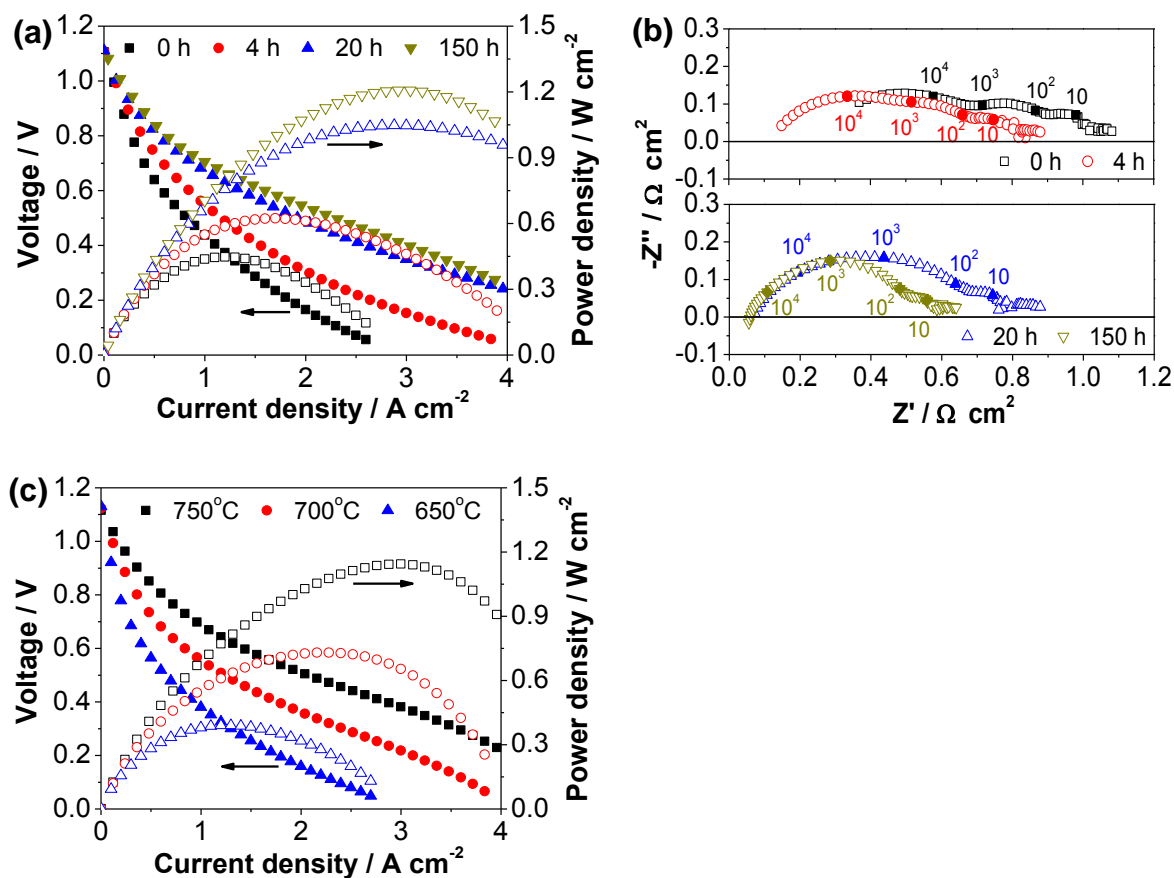
21
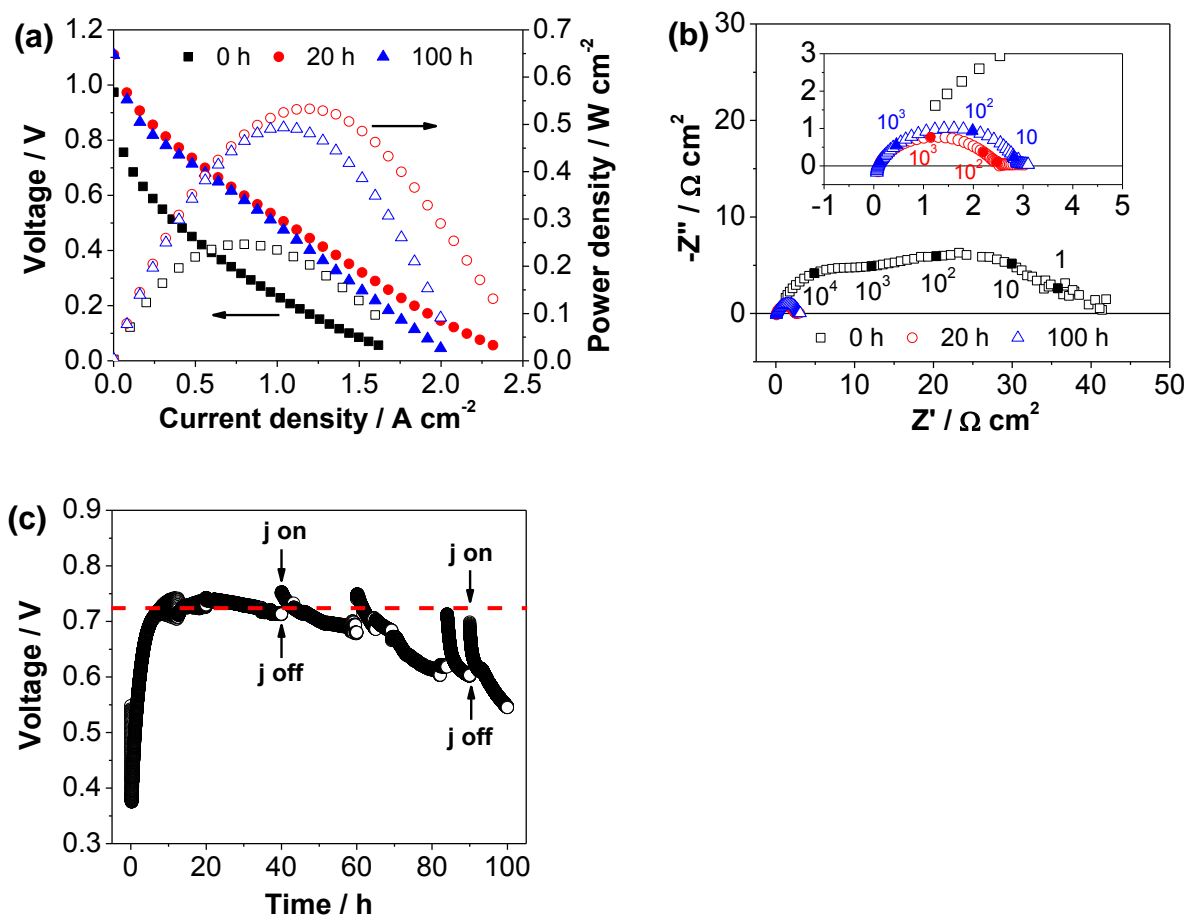
**Figure 2**. Polarization curves and impedance spectra of a cell with directly assembled LC cathode at 750 °C: (a) polarization curves as a function of polarization time at 500 mA cm$^{-2}$, (b) impedance spectra measured at open circuit and numbers are frequencies in Hz, and (c) stability curve at 500 mA cm$^{-2}$. The stability tests were interrupted from time to time to measure the polarization curves and impedance spectra.

**Figure 3**. Polarization curves and impedance spectra of a cell with directly assembled LC-GDC composite cathode at 750 °C: (a) polarization curves as a function of polarization time at 500 mA cm$^{-2}$, (b) impedance spectra measured at open circuit and numbers are frequencies in Hz. (c) Polarization curves measured at different temperatures; in this case, a new cell with directly assembled LC-GDC composite cathode was used and polarized at 500 mA cm$^{-2}$ and 750 °C for 20 h before the measurement of polarization performance.

23
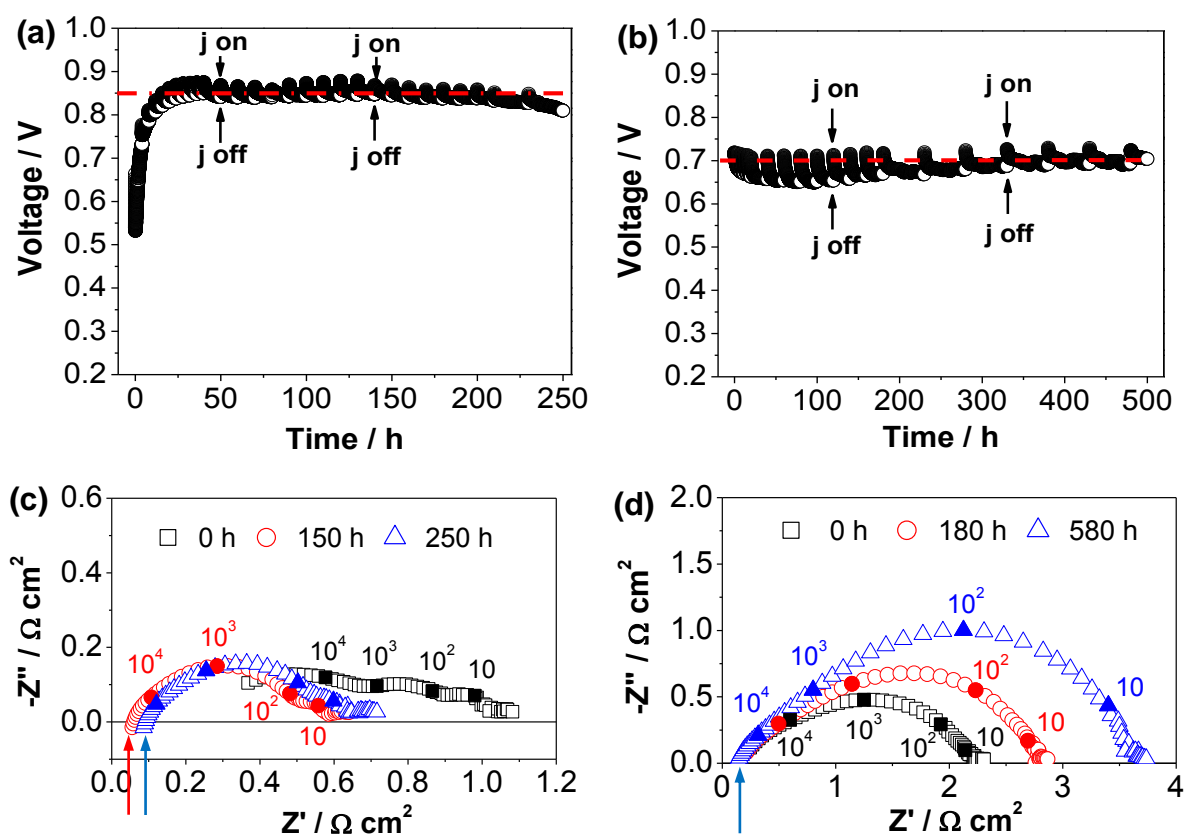
**Figure 4**. Stability curves and impedance spectra of cells with directly assembled LC-GDC composite cathodes: (a,c) at 500 mA cm$^{-2}$ and 750 $^{o}$C and (b,d) at 250 mA cm$^{-2}$ and 650 $^{o}$C. Numbers in the impedance spectra are frequencies in Hz. Different cells were used for the stability tests at 750 and 650 $^{o}$C.
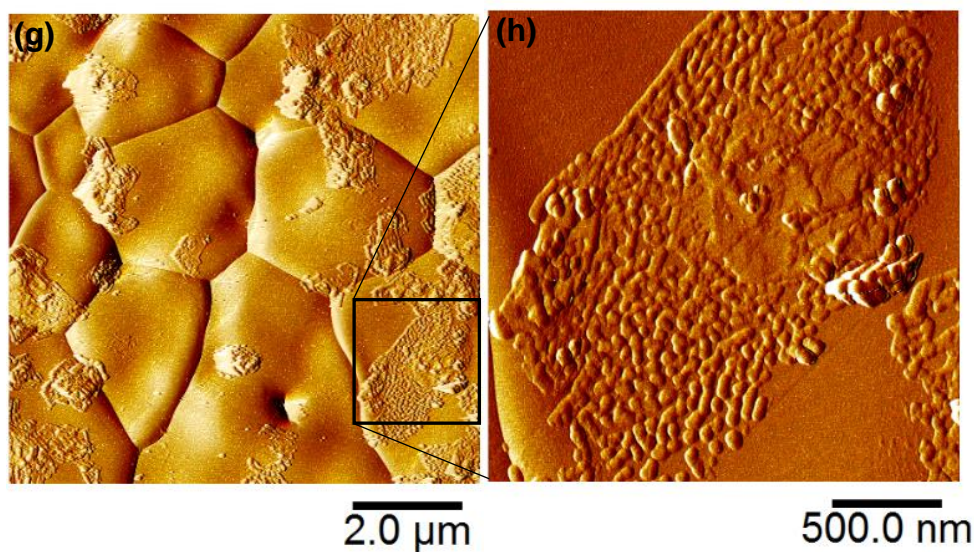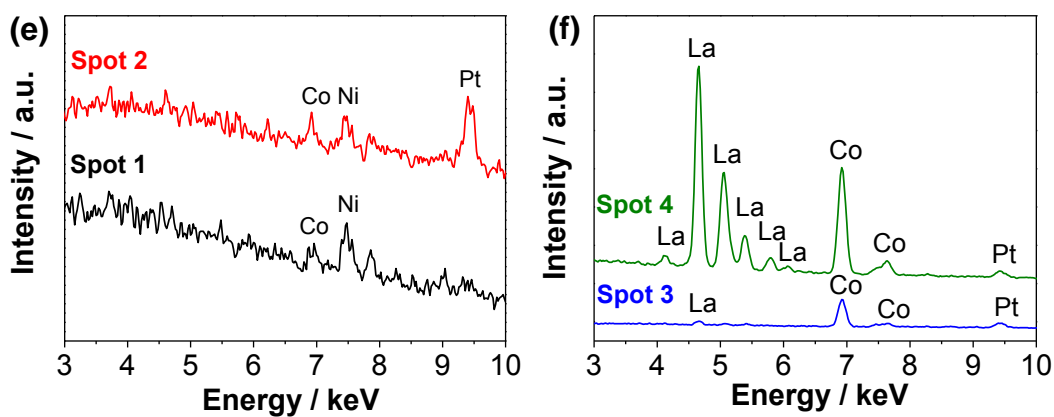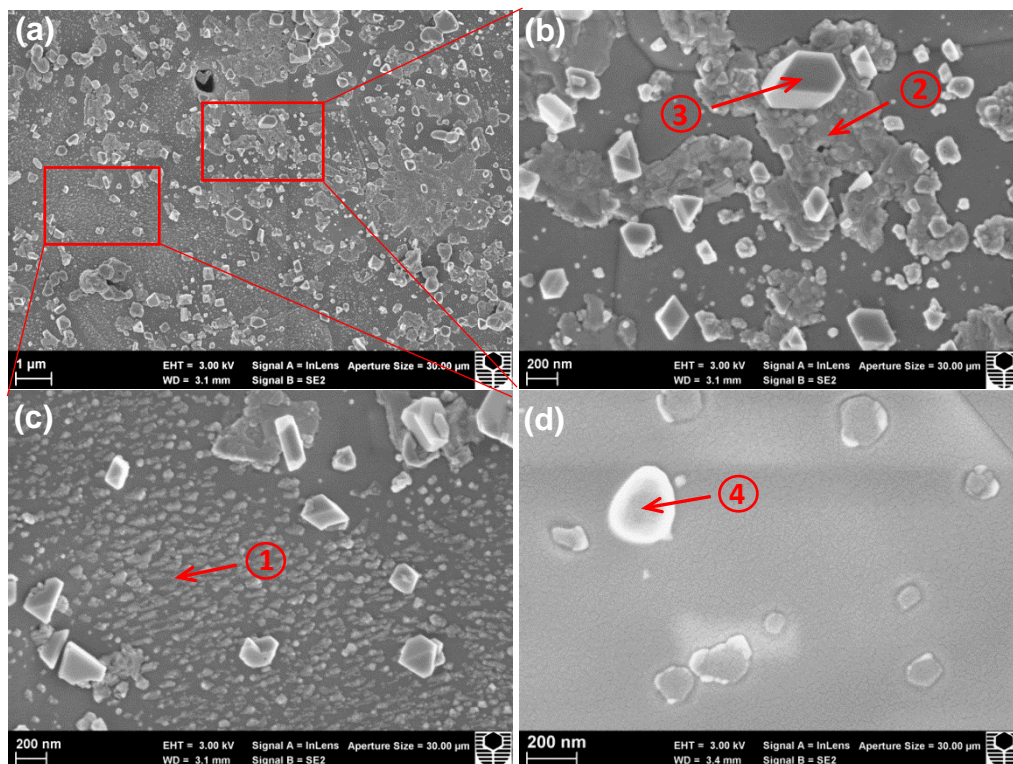
**Figure 5**. SEM micrographs of YSZ electrolyte surface after polarization at 500 mA cm$^{-2}$, 750 $^{\circ}$C for 100 h and removal of LC electrode by adhesive tape: (a) overview and (b,c) enlarged views. (d) YSZ electrolyte surface after heat-treatment at 750 $^{\circ}$C for 250 h under open circuit. (e,f) EDS spectra of selected spots. (g,h) AFM micrographs of acid cleaned YSZ electrolyte surface after polarization at 500 mA cm$^{-2}$ and 750 $^{\circ}$C for 12 h.

26
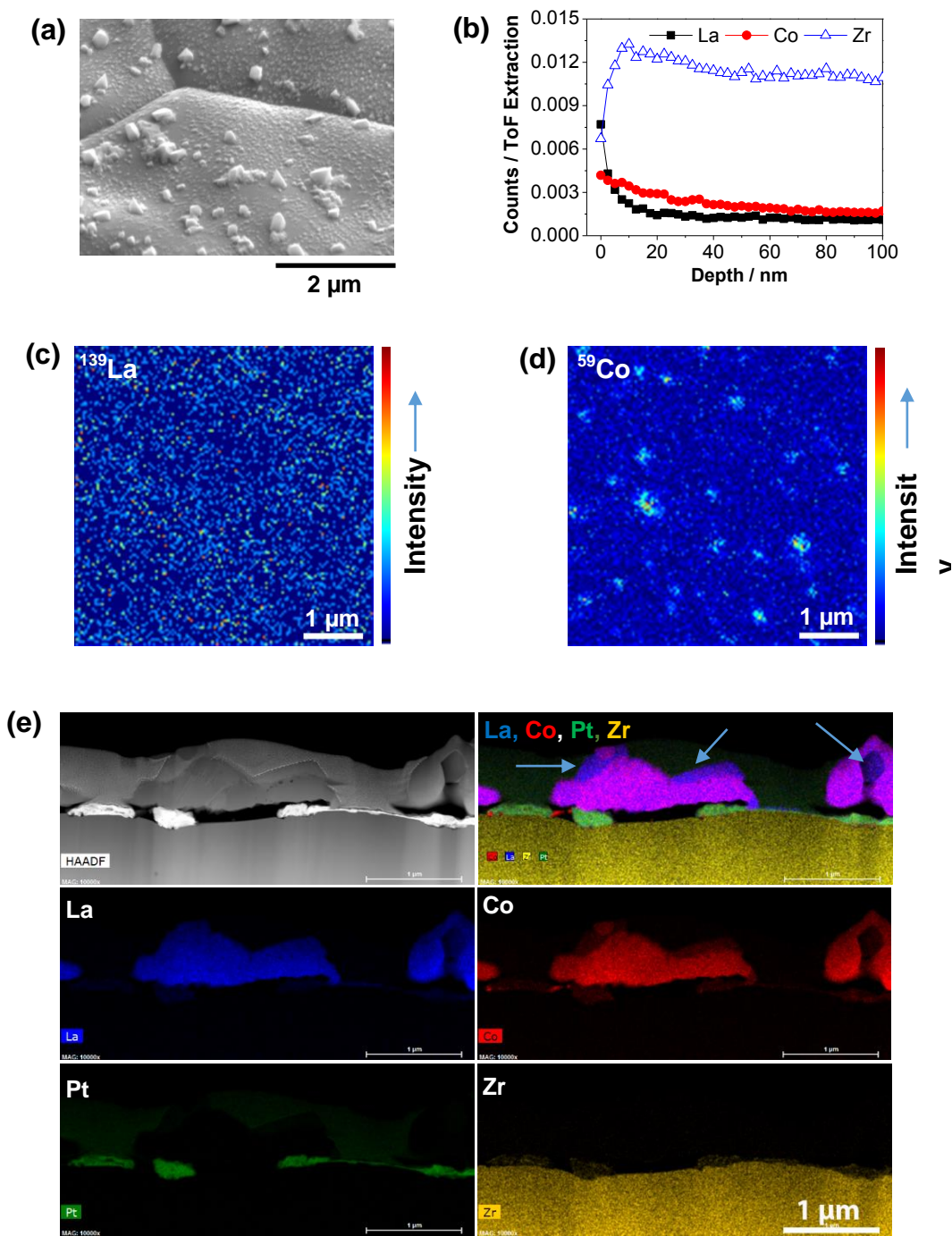
**Figure 6**. (a) SEM micrograph of YSZ electrolyte surface (the stage was tilted on the y-direction and the scale bar is only for the x-direction), (b) SIMS depth profiles, and (c.d) La and Co SIMS maps of the YSZ surface (approx. top 10 nm and 50 nm, respectively), and (e) STEM image and elemental maps at the LC cathode/electrolyte interface, after the directly assembled LC electrode was polarized at 500 mA cm$^{-2}$, 750 $^o$C for 100 h.

27

**Figure 7**. (a) SEM micrograph of cross section of the cell with directly assembled LC-GDC electrode after polarization at 500 mA cm$^{-2}$, 750 $^o$C for 250 h. (b) SEM and (c,d) AFM micrographs of the YSZ electrolyte surface after polarization for 40 h, and (e) height analysis of selected contact rings as indicated in (c). In (c-d), the LC-GDC electrode was removed by HCl treatment.
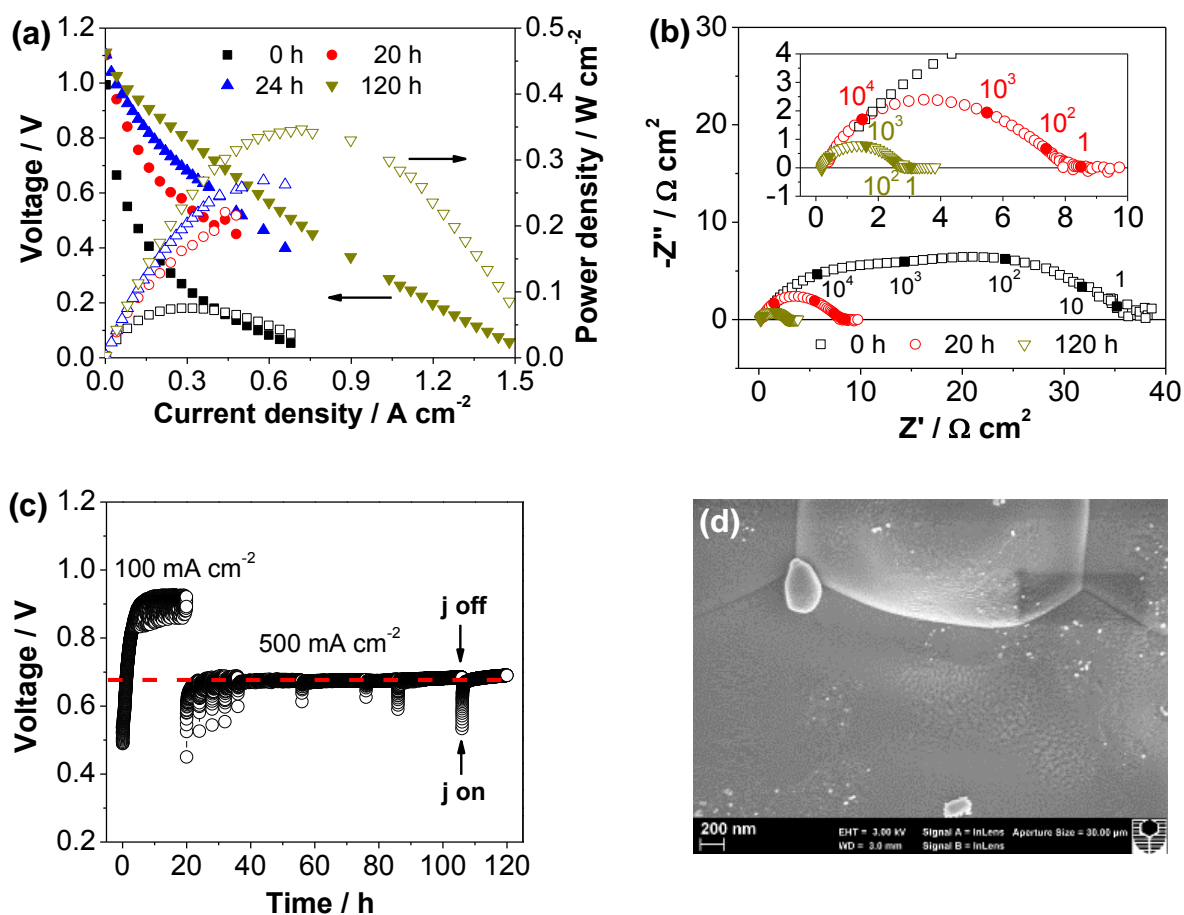
**Figure 8**. Polarization curves and impedance spectra of a cell with directly assembled SmC cathode at 750 $^o$C: (a) polarization curves after polarization at 100 mA cm$^{-2}$ for 20 h and 500 mA cm$^{-2}$ for 24 and 100 h, (b) impedance spectra measured at open circuit and numbers are frequencies in Hz, and (c) stability curve at 100 mA cm$^{-2}$ and 500 mA cm$^{-2}$. The stability tests were interrupted from time to time to measure the polarization curves and impedance spectra. (d) SEM micrograph of YSZ electrolyte surface in contact with the directly assembled SmC cathode after polarization at 750 $^o$C for 120 h.

29
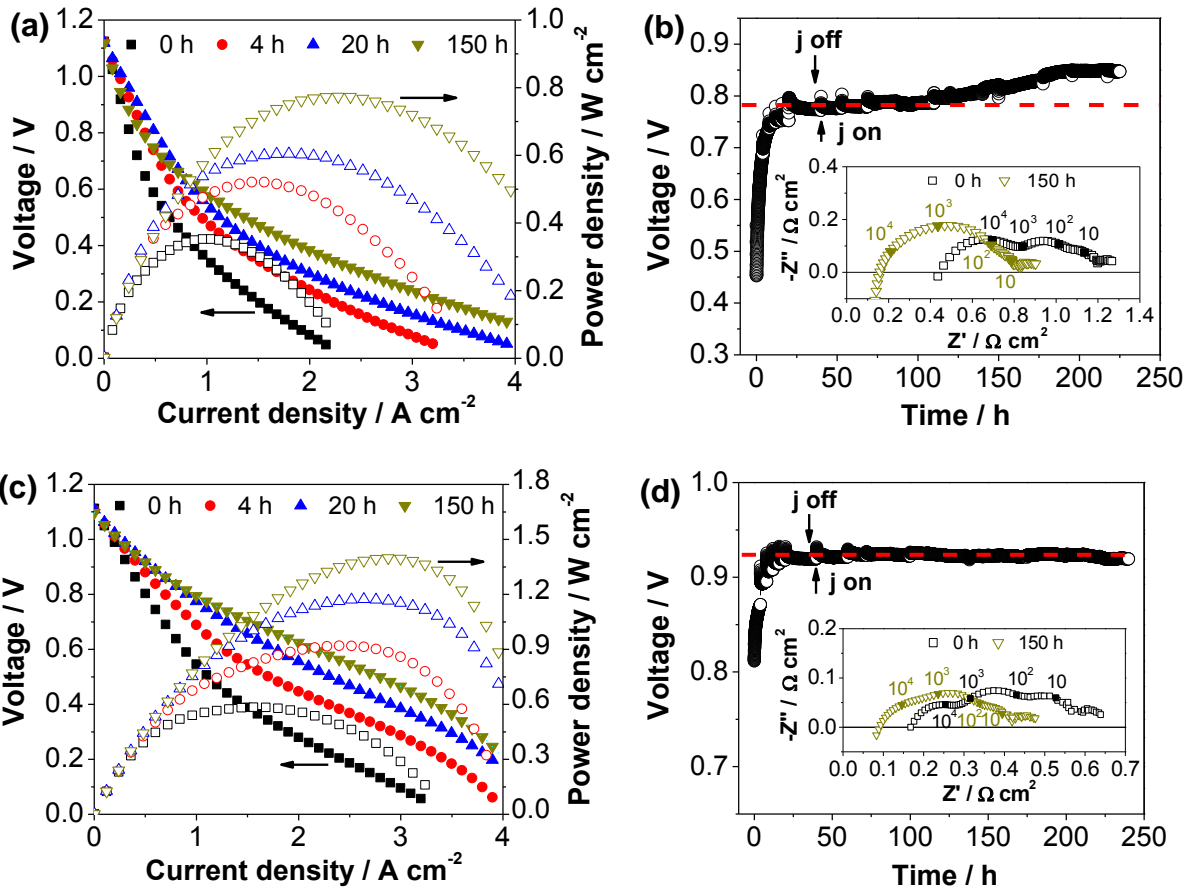
**Figure 9**. Polarization performance of cells with directly assembled (a,b) SmC-GDC and (c,d) SmCPd-GDC composite cathodes at 750 °C: (a,c) polarization curves as a function of polarization time at 500 mA cm$^{-2}$ and (b,d) cell voltage recorded at 500 mA cm$^{-2}$. The insets in (b,d) are impedance spectra measured at open circuit and numbers are frequencies in Hz. The stability tests were interrupted from time to time to measure the polarization and impedance curves.
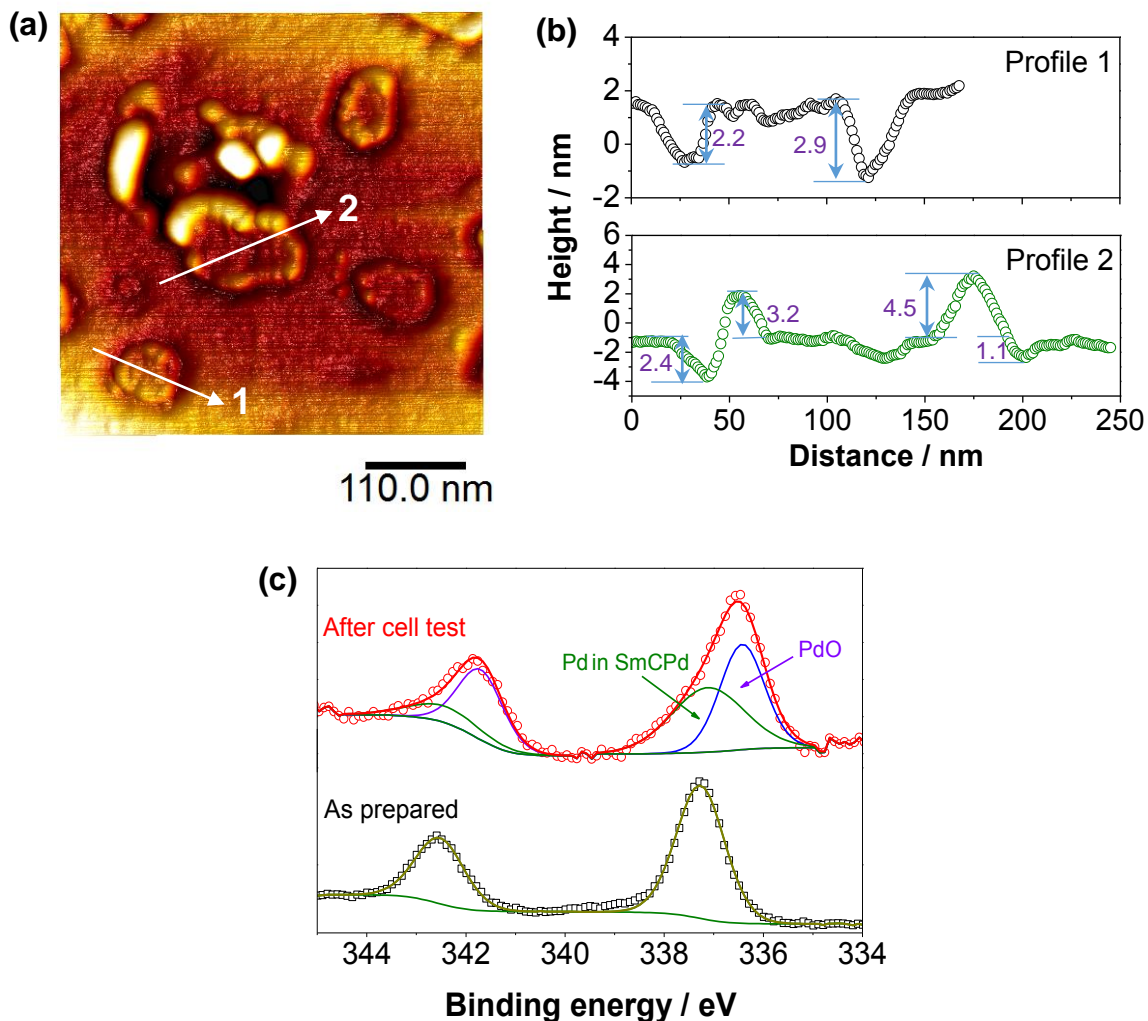
30

**Figure 10.** (a) AFM micrograph and (b) height profiles of selected contact marks on YSZ electrolyte surface in contact with directly assembled SmCPd-GDC cathode after polarization at 500 mA cm$^{-2}$ and 750 $^o$C for 240 h. The electrode was removed by HCl treatment. (c) XPS core levels of Pd 3d of SmCPd-GDC electrodes before and after polarization at 500 mA cm$^{-2}$ and 750 $^o$C for 160 h.

31

# Electronic Supporting Information

# Highly stable Sr-free cobaltite based perovskite cathodes directly assembled on barrier-layer-free Y₂O₃-ZrO₂ electrolyte of solid oxide fuel cells

Na Ai,‡[a,b] Na Li,‡[c] William D.A. Rickard,[d] Yi Cheng,[b] Kongfa Chen,[*,a,b] and San Ping Jiang[*b]

[a] College of Materials Science and Engineering, Fuzhou University, Fuzhou, Fujian 350108, China

[b] Fuels and Energy Technology Institute and Department of Chemical Engineering, Curtin University, Perth, WA 6102, Australia

[c] College of Science, Heilongjiang University of Science and Technology, Harbin 150022, China

[d] John De Laeter Centre & Department of Physics and Astronomy, Curtin University, Perth, WA 6102, Australia

[*] Corresponding author. Tel.: +61 8 9266 1723; fax: +61 8 9266 1138.
*Email address*: chenkongfa@gmail.com (K. Chen).
[*] Corresponding author. Tel.: +61 8 9266 9804; fax: +61 8 9266 1138.
*Email address*: S.Jiang@curtin.edu.au (S.P. Jiang).
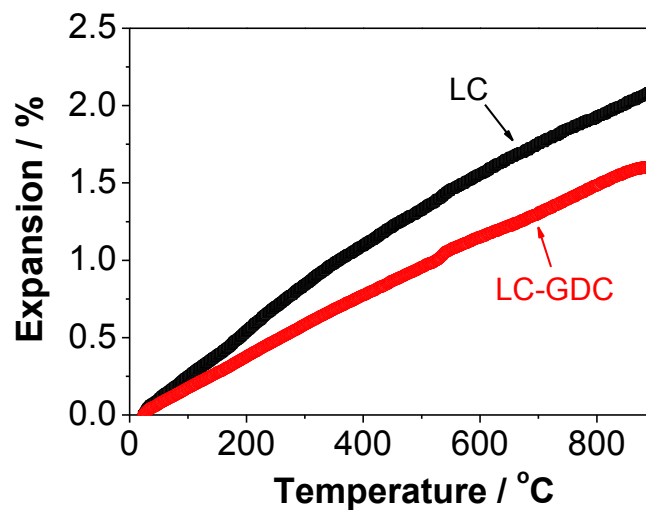‡These authors contributed equally.

**Figure S1**. Thermal expansion plots of pristine LC and LC-GDC (6/4, w/w) composite bar samples.
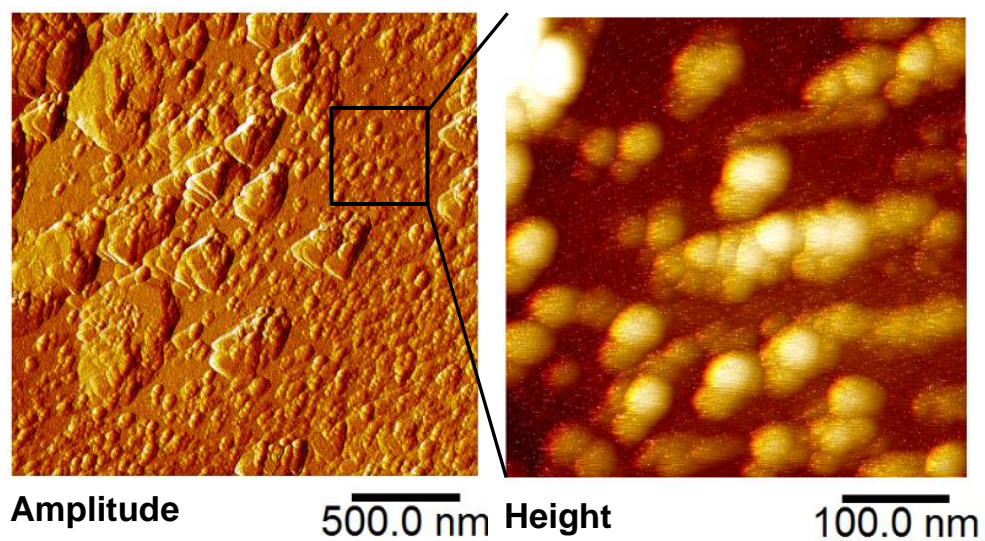
**Figure S2**. AFM images of YSZ surface in contact with directly assembled LC electrode after polarization at 500 mA cm$^{-2}$, 750 $^{o}$C for 100 h. LC electrode was removed by acid treatment.
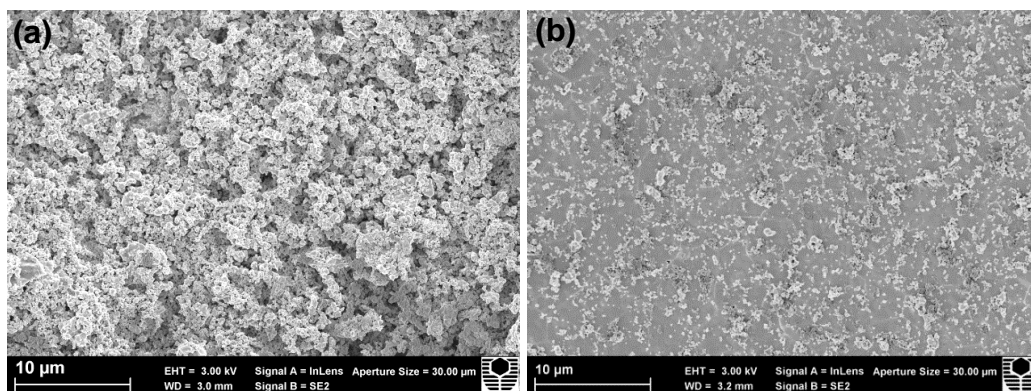
3

**Figure S3**. YSZ electrolyte surface in contact with directly assembled LC-GDC electrode after heat-treatment at 750 $^{\circ}$C for 250 h. (a) under cathodic polarization at 500 mA cm$^{-2}$ and (b) under open circuit.
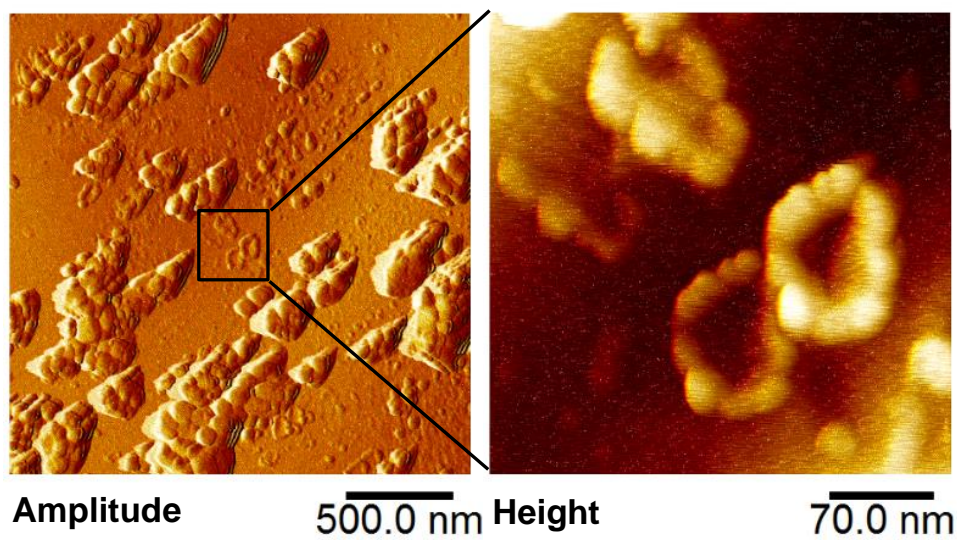
**Amplitude**     500.0 nm **Height**     70.0 nm

**Figure S4**. AFM images of YSZ electrolyte surface in contact with directly assembled LC-GDC electrode after polarization at 250 mA cm$^{-2}$, 650 $^o$C for 500 h. LC-GDC electrode was removed by acid treatment.

5